doi:10.3788/gzxb20154405.0516001

双原子正方晶格光子晶体边界模式的光传输特性

王道斌,元丽华,雷景丽, 李晓晓, 侯尚林
(兰州理工大学 理学院, 兰州 730050)

摘 要:利用平面波展开法,发现双原子正方晶格光子晶体中 ΓM 方向边界面存在着快慢两类边界模式,并且通过计算色散关系和电场分布研究了边界参量对这两类边界模式传输特性的影响.依据两种模式的色散关系,计算了群指数和群速度色散参量,结果表明边界参量的变化对第一类边界模式传输特性的影响较小,该模式的平均群指数始终维持在 5.0 左右;第二类边界模式与第一类模式明显不同,边界参量的变化能够有效地影响到这种模式的传输特性,该模式的最大平均群指数可达 178 左右.利用时域有限差分法记录了不同时刻电场强度在边界附近的分布及监测点处的电场幅度变化情况,结果表明,两类模式都能够被限制在边界附近并向前传播,时域有限差分法得到的群速度与平面波展开法的结果完全吻合.

关键词:纳米光子学; 光子器件; 时域有限差分法; 双原子光子晶体; 表面波; 光子带隙; 慢光; 群速度色散; 光存储

中图分类号:O481.1; O472.3 **文献标识码**:A **文章编号**:1004-4213(2015)05-0516001-7

Light Propagation and Localization Properties of Edge States in Diatomic Square Lattice

WANG Dao-bin, YUAN Li-hua, LEI Jing-li, LI Xiao-xiao, HOU Shang-lin
(*School of Science, Lanzhou University of Technology, Lanzhou* 730050, *China*)

Abstract: Utilizing the plane wave expansion method, it is found that there are two types of edge states existing on the surface termination along the ΓM direction of a diatomic photonic crystal. Through analying the surface mode band structure and the field distribution, the effect of the edge parameter on the waveguiding properties of these edge states were investigated. The group index and group velocity dispersion parameter were calculated according to the dispersion curves. The results demonstrate that the variation of the edge parameter has a very slight effect on the light propagation properties of first type of edge state. Its average group index is always around 5.0. The second edge state is obviously different with the first state and the variation of edge parameters can control the propagation performance of this mode efficiently. The maximal average group index of this edge state can achieve 178. The finite difference time domain methods was used to record the electric field distributions and amplitudes near the surface at different times. From the obtained results, it is found that these edge states can be confined in the area near the surface termination and propagate forward. The group velocity extracted from the finite difference time domain method is consistent with the result from the plane wave expansion method.

Key words: Nanophotonics; Photonic devices; Finite difference time domain method; Diatomic square lattice; Surface waves; Optical band gaps; Slow light; Group velocity dispersion; Optical memories

OCIS Codes: 160.5298; 240.6690; 130.5296; 130.3120; 210.4680

Foundation item: The National Natural Science Foundation of China (Nos. 61367007, 61167005), the Natural Science Fund of Gansu Province of China (Nos. 1112RJZA017, 1112RJZA018) and the Research Fund for the Doctoral Program of Lanzhou University of Technology

First author: WANG Dao-bin (1976—), male, lecturer, Ph. D degree, mainly focuses on nanophotonics and optical communication technology. Email: photonics_wang@yahoo.com

Received: Jul. 22, 2014; **Accepted**: Jun. 27, 2015

0 Introduction

The surface electromagnetic waves can reside at the interface between Photonic Crystal (PhC) and open space due to the confinements of total internal reflection and photonic bandgap effects[1]. Unlike the surface plasmonic wave in metallic surface, the Bloch surface wave in dielectric PhC surface exhibits no intrinsic radiation loss and infinite lifetime, which could provide efficient light matter interactions for various optical devices[2, 3]. In recent years, this phenomenon has attracted much research interest from both industry and academic community in view of its potential application scope. Based on the surface states in photonic crystals, the waveguide components with directional emissions[4-5] and efficient coupling[6-8] have been proposed and demonstrated, which are the very essential parts of future photonic integrated circuits. Meanwhile, some studies have shown that, if the translational symmetry along the boundary of the semi-infinite photonic crystal is broken, the surface mode will turn into a resonant state with a finite lifetime, which can be utilized for optical filters[9-10], lasers[11-12], sensors[13], and so on. Recently, there has been growing interest in exploring the light propagation property of photonic crystal surface modes[14-16].

The diatomic square lattice is bipartite, meaning that it has two lattice sites per unit cell and can be called polyatomic photonic crystal[15,17]. Compared with the monoatomic photonic crystal, the polyatomic photonic crystal presents some kinds of advantage and the extensive research work is really needed to investigate the wave transport phenomena for it. In Ref. [18], authors have investigated the dispersion and modal symmetries of the edge states along the ΓX direction supported by diatomic square lattice. But, to our best knowledge, no existing research addresses the light propagation phenomenon at the edge along the ΓM direction of diatomic square lattice until now. In this work, we theoretically study the light propagation at the edges of a diatomic photonic crystal based on square lattice, especially for the ΓM direction. All results have also been verified by the Finite Difference Time Domain (FDTD) method.

1 Model structure of surface

The diatomic square lattice investigated throughout this work can be generated by the overlay of the square lattice B with dielectric rods of radius r on top of the square lattice A with dielectric rods of radius R, as shown in Fig. 1 (a). These two sublattices have the same lattice constant a, but the dielectric rods of lattice B are placed in the center of each cell of square lattice A. This arrangement forms a primitive cell containing two different scatter elements, which are a large rod at the center of the cell and a small rod distributed as four quadrants at the corners of the cell. In this paper, the rod radii of the sublattices are $0.28a$ and $0.12a$, respectively, where a is the lattice constant and the rods are made of a material with refractive index 3.464 1. Fig. 1 (b) shows the calculated band diagram for the diatomic square lattice with no edges. It can be found that the photonic crystal geometry investigated in this paper exhibits a band-gap for TE like modes between $\omega_{\min}=0.237\ 4\ (2\pi c/a)$ and $\omega_{\max}=0.278\ 7\ (2\pi c/a)$.

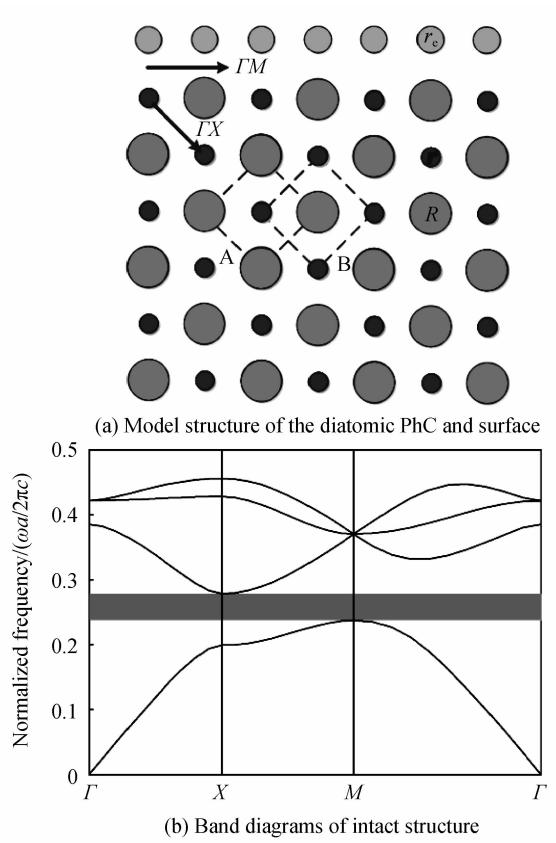

Fig. 1 Schematic picture of the diatomic photonic crystal geometry and its band diagram

2 Results from the plane wave expansion method

There are two types of edge in the diatomic photonic crystal based on square lattice: the edge along the ΓX direction and the edge along the ΓM direction. In this paper, we will focus our attention on the guiding properties of the surface along the ΓM direction. For the investigated diatomic photonic crystal, the edge states can only exist in truncated photonic crystal with the surface perturbed in some way. We consider the surface termination that has translational symmetry along the surface and the dielectric rods at the edge are modified to have identical

radius, as shown in Fig. 1 (a). In this figure, the radius of the edge rods is denoted by r_e.

Fig. 2 (a) shows the dispersion of edge states of the surface termination shown in Fig. 1 (a), calculated by the Plane Wave Expansion (PWE) method using MIT's freely available software MPB[19]. The radius of the edge rods is $r_e = 0.19a$. In the evaluation of the edge states, we assumed the PhC stripe of $N = 27$, being N the number of the layers along the direction perpendicular to the edge direction and set our computational cell to be a $\sqrt{2}\,a \times 25\sqrt{2}\,a$ supercell. Periodic boundary conditions are imposed in both directions. From this plot, the investigated edge can provide two surface modes in the frequency region of interest. Mode A is shown by a red solid line, whereas mode B is represented by a blue solid line in this figure. Field distributions for the corresponding edge modes are given in Fig. 2 (b) and Fig. 2 (c). We can find that the optical fields of two modes are all confined to the edge rods, but there are obvious differences in the distribution patterns of electric field. For the mode B, the distribution pattern is simple and the strongest field intensity is found in the center of the edge rods, whereas the distribution pattern of mode A is complex and the optical field energy spread in different edge rods.

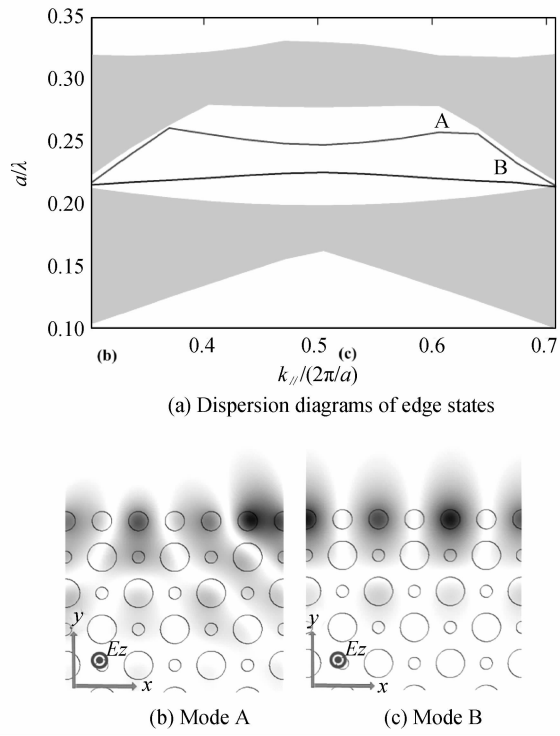

Fig. 2 Calculated dispersion and electric field of edge states for the structure shown in Fig. 1 at $k_{//} = 0.45(2\pi/a)$

The surface mode band structure and the field localization highly depend on the edge parameters. So controlling the propagation performance of the edge modes by subtle structural modification should be examined comprehensively. In order to investigate the impact of radius r_e on the dispersion curve of these two edge modes and how the flat band moves with different values of r_e, we have analyzed the optical characteristics of this surface termination for a range of the radius r_e from $0.19a$ to $0.23a$. Fig. 3 shows the projected dispersion diagrams of these two edge modes for the different values of r_e. While r_e is varied from $0.19a$ to $0.23a$ with an incremental step of $0.01a$, the guided surface modes all move downwards in the frequency axis as expected, but the variation of the dispersion curve slope is quite different for these two modes. For mode A, the slope of the dispersion curve has almost no change with the variation of the radius r_e. However, there is significant change in the slope of the dispersion curve of mode B and the slope signs change from positive to negative when $k_{//}$ is less than $0.5(2\pi/a)$.

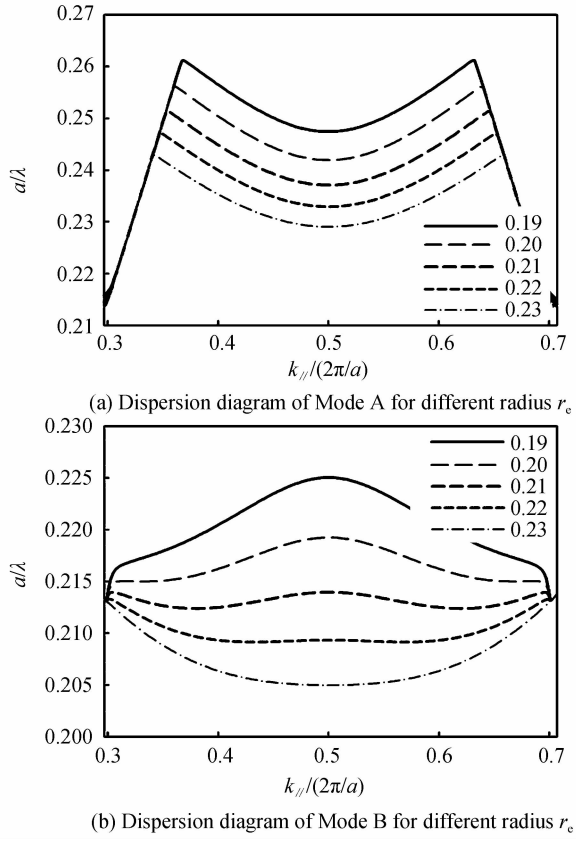

Fig. 3 Projected dispersion diagram of edge states for different radius r_e

The group velocity, $v_g = \partial\omega(k)/\partial k$, is calculated using the Hellman-Feynmann theorem, and then the group index n_g can be obtained as[20]

$$n_g = c/v_g = c\mathrm{d}k/\mathrm{d}\omega \quad (1)$$

where c is the light velocity in vacuum and v_g is the group velocity of the edge states. The related n_g curves with normalized frequency under different values of r_e are displayed in Fig. 4. The calculated n_g curves of

mode A are L-shaped at the different values of r_e. The n_g curve of mode B is still L-shaped at $r_e=0.19a$, but it converts to U-shaped when r_e takes the other values. This figure clearly illustrates the influence of radius r_e on the waveguiding properties of these two surface modes. The variation of radius r_e has a very slight effect on the light propagation properties of mode A, whose modulus of the group index n_g and the corresponding bandwidth have almost no change when r_e is increased from $0.19a$ to $0.23a$. The variation tendency of n_g curves of mode B is obviously different with that of mode A.

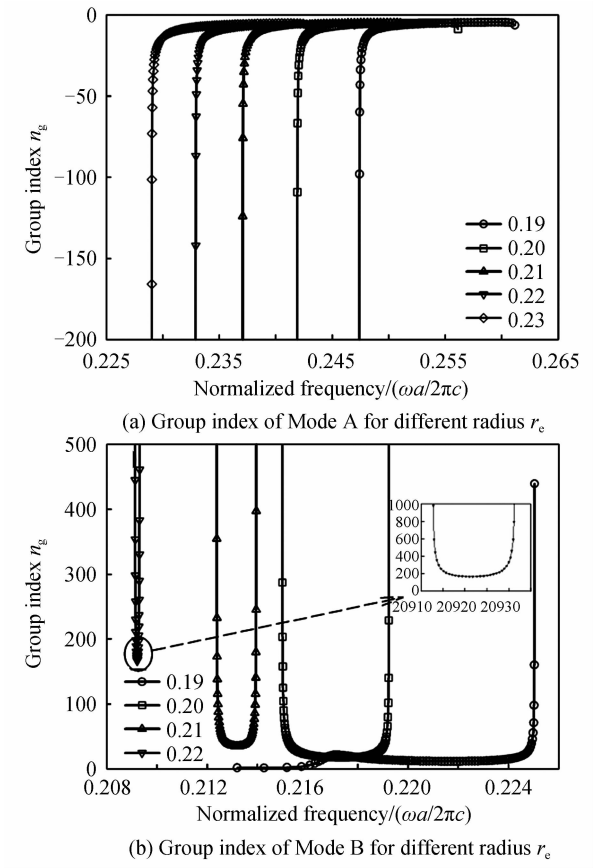

Fig. 4 Group index variation of edge states versus normalized frequency for different radius r_e

From Fig. 4 (b), we can find that the corresponding modulus of the group index n_g of mode B increases significantly with r_e, but the available bandwidth decreases when r_e increases. In other words, the subtle modification of edge parameters can control the propagation performance of the mode B efficiently. Because the slope sign is negative, so the Fig. 4 (b) doesn't display the calculated n_g curves of mode B at $r_e=0.23a$.

Group Velocity Dispersion (GVD) effect of surface modes, which can cause pulse broadening and signal distortion, is characterized by the GVD parameter in our works. It can be calculated as Eq. (2) and the results have been shown in Fig. 5. Form this plot, the calculated β_2 curves of mode A are also L-shaped and gradually translate toward the lower frequency part with increasing the radius r_e. For mode B, the values of β_2 drop from positive GVD more than $3\times10^6(a/2\pi c^2)$ to negative GVD less than $-3\times10^6(a/2\pi c^2)$ by several orders of magnitude when r_e is increased from $0.19a$ to $0.23a$. The minimal GVD exists at the middle region, while corresponding group velocity also comes to bigger value here. So, minimizing the GVD effect and slowing the group velocity are two sides of the coin. One can chooses feasible slow light regions according to the practical application requirement.

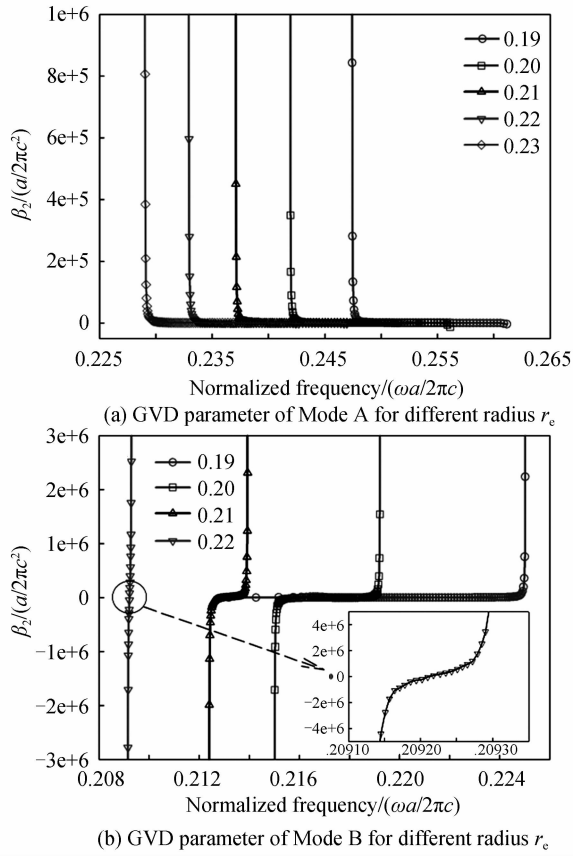

Fig. 5 GVD parameter of edge states versus normalized frequency for different radius r_e

$$\beta_2=\partial^2 k/\partial\omega^2 \tag{2}$$

In order to examine the optical characteristics of the edge states more clearly, we extract the average group index and corresponding bandwidth value with different radius r_e from Fig. 4. The average group index is evaluated by[21]

$$\tilde{n}_g=\int_{\omega_0}^{\omega_0+\Delta\omega} n_g(\omega)\,\mathrm{d}\omega/\Delta\omega \tag{3}$$

where $\Delta\omega$ represents the bandwidth of slow light, which is defined as the wavelength range corresponding to a maximum of 10% n_g variation with respect to the average group index. The corresponding results for different values of r_e have been shown in Table 1. These results also demonstrate that the variation of radius r_e has a very small influence on the light

propagation properties of mode A. The average group index and the corresponding bandwidth of mode A almost keep unchanged when the radius r_e increases. For mode B, the bandwidth higher than 0.0044 ($2\pi c/a$) and the average group index higher than 177.57 can be obtained. The Normalized Delay Bandwidth Product (NDBP), another key parameter for slow light performance, is defined as the product of the average group index and bandwidth[22]. The corresponding results are also shown in Table 1. When r_e is increased from $0.19a$ to $0.23a$, the maximum NDBP is calculated to be 0.1732 and 0.2446 for these two edge modes, respectively.

3 Results from the finite difference time domain method

The slow light excitation and propagation at the edge along the ΓM direction of diatomic square lattice have also been simulated by using the finite difference time domain method[23]. The surface termination with a total length $L=80a$ and the radius $r_e=0.20a$ has been chosen to verify the results in the frequency domain calculation of the photonic bands. Perfectly Matched Layers (PML) are applied to the surroundings of the structure to inhibit the reflections coming from the boundaries of the computational domain. A Gaussian pulse source, with a frequency width of $\Delta\omega=0.0003$ ($2\pi c/a$), is placed at the upper left side of the structure to excite the surface modes. For mode A, the Gaussian source is centered at 0.244387 ($2\pi c/a$). In case of mode B, the center frequency of the Gaussian source is shifted to 0.218149 ($2\pi c/a$). Fig. 6 shows the normalized pulse shapes detected by the input and output time monitors placed at the two sides of the

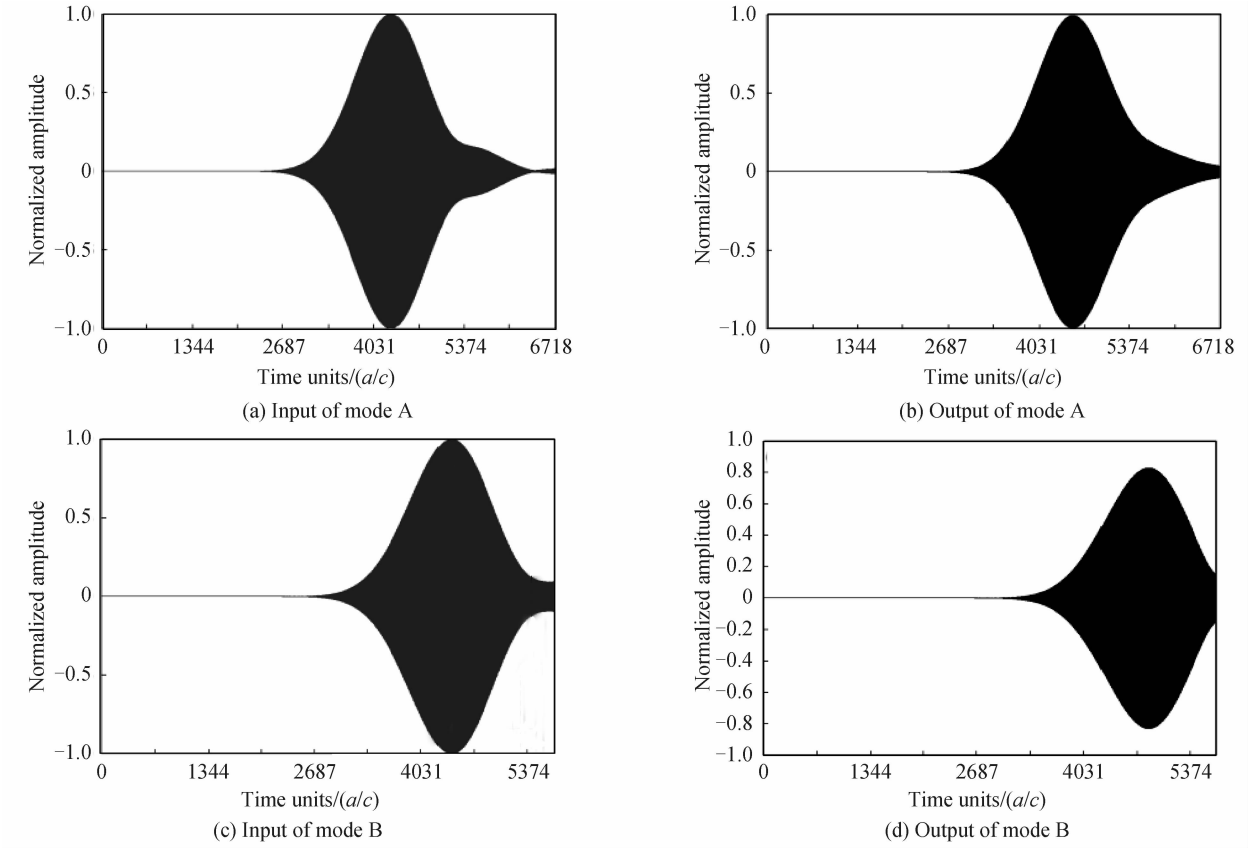

Fig. 6 Temporal presentations of the optical pulses at the input and the output detecting points for edge states

surface termination. The distances between the input and output time monitors are different for mode A and mode B. In Fig. 6 (a) and (b), the initial pulse and the pulse after traveling propagation distance of $L_d=30a$ are shown for mode A. The same comparison is performed for mode B in Fig. 6 (c) and (d), but the traveling propagation distance is set to $L_d=20a$. The group index can be obtained by dividing the delay time between the two peaks by the transmission length. From Fig. 6 (c) and (d), the peaks of mode B are located at 4420.4 (a/c) and 4850.5 (a/c) in the input and output detecting points, respectively. The total time delay between the two peaks of mode B in Fig. 6 is approximately $t_d=430$ (a/c). Thus, the calculated n_g according to the FDTD simulations is $n_g=t_d/L_d\approx 21.5$, which deviated slightly from the result of $n_g=18.9$ obtained by the PWE calculation. Similar comparison and conclusion can be made in case of mode A. In Fig. 6 (c) and (d), the peak value of the output pulse is slightly reduced compared with that of the

input pulse, but no obvious reduction in the peak amplitude of the output pulse is observed In Fig. 6 (a) and (b). The same phenomenon can also be found in Fig. 7, which shows the FDTD simulated electric field distributions across the surface termination of these two modes. This phenomenon is mostly due to the fact that the dispersion curve of mode B is closer to the dielectric band than that of the mode A. So, the field energy of mode B can easily diffuse into the interior of the photonic crystal, which degrades the peak amplitude of the output pulse in Fig. 6 (d) and Fig. 7 (b).

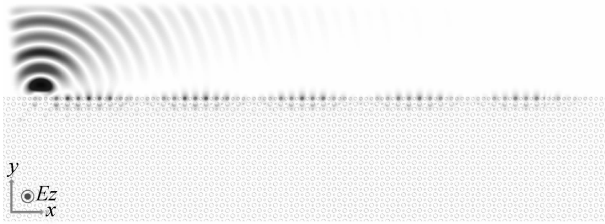

(a) Electric field distributions of mode A in the surface termination

(b) Electric field distributions of mode B in the surface termination

Fig. 7 FDTD simulated electric field distributions of edge states in the surface termination

Table 1 Bandwidth, average group index and NDBP for edge states

Mode A			
r_e	Bandwidth ($\omega a/2\pi c$)	Average Group Index	NDBP
$0.19a$	7.8×10^{-3}	−4.9747	0.151 0
$0.20a$	8.0×10^{-3}	−5.006 0	0.159 0
$0.21a$	7.8×10^{-3}	−5.170 4	0.163 2
$0.22a$	7.8×10^{-3}	−5.397 5	0.173 2
$0.23a$	7.2×10^{-3}	−5.630 1	0.169 5
Mode B			
r_e	Bandwidth ($\omega a/2\pi c$)	Average Group Index	NDBP
$0.19a$	4.4×10^{-3}	12.314 4	0.244 6
$0.20a$	2.1×10^{-3}	18.712 8	0.180 8
$0.21a$	8.0×10^{-4}	36.397 0	0.136 6
$0.22a$	1.0×10^{-4}	177.570 3	0.084 9

Finally, we investigated the attenuation of surface electromagnetic wave in horizontal and vertical directions. In order to measure the amplitude of surface wave propagating in the horizontal direction, three time monitors have been deliberately placed along the surface termination of photonic crystal. The first monitor was positioned at $12a$ behind the Gaussian source. The second and third monitors were positioned at $20a$ and $30a$ behind the first monitor, as shown by the inset of Fig. 8 (a). All electric field amplitudes have been normalized by the measured value of the first monitor and the obtained results have been shown in Fig. 8 (a). For this figure, we can find that the mode A has a low attenuation coefficient and it can keep the stable field amplitude between the first and third monitors. But the mode B shows an obvious reduction in the field amplitude, compared with the mode A. In order to record the attenuation of surface wave in the vertical direction, three time monitors have also been placed the direction perpendicular to the surface termination. The first monitor was located just at the surface termination. The vertical distances from the first monitor to the second and third monitors were $1.0a$ and $1.5a$, as shown by the inset of Fig. 8 (b). The results shown in Fig. 8 (b) illustrate that these two modes decay with the large attenuation coefficient in the vertical direction. About in the distance of $1.5a$, the field amplitude of mode A is reduced to nearly one-third of its original value.

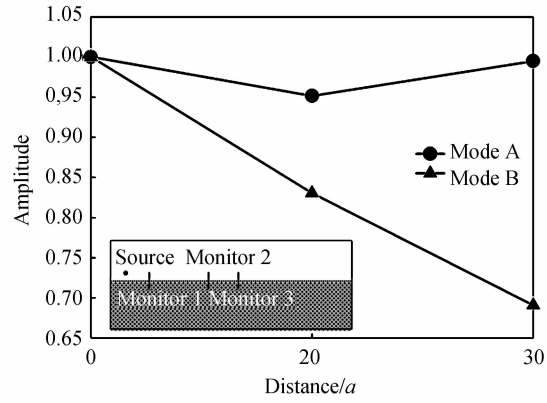

(a) Attenuation of surface wave in horizontal direction

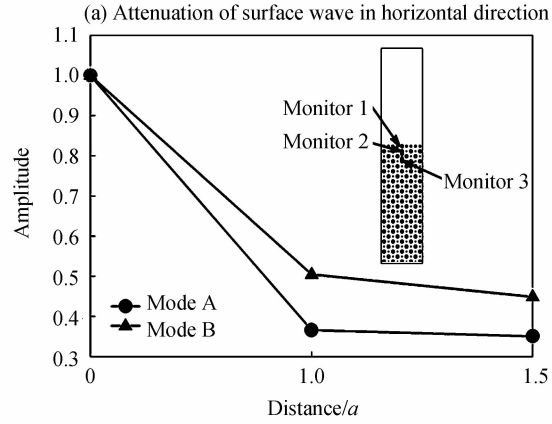

(b) Attenuation of surface wave in vertical direction

Fig. 8 The amplitude variation of surface electromagnetic wave in horizontal and vertical directions

Except for the edge along the ΓM direction, we also have investigated the waveguiding properties of the edge along the ΓX direction. The results show that the surface termination along the ΓX direction can only provide one edge state in the frequency region of

interest and there is no mode whose field distribution is similar with Fig. 2 (b). So, we can conclude that the mode A above mentioned is unconventional and the mechanism underlying its formation should be inquired carefully. Although the modulus of the average group index of mode A is small, its value always maintains at 4.9～5.6 shown in Table 1 and is almost free from the effects of radius r_e, which maybe means that this mode can hardly suffer from the fabrication imperfections. More smart and effective optimization methods can also be explored to enhance the propagation performance of mode A.

4 Conclusion

In summary, the existence of localized edge states in the diatomic square lattice with perturbations made to the radius of edge rods are investigated theoretically. Electromagnetic analysis via PWE and FDTD numerical techniques are employed to calculate band structures, spatial mode profiles and optical propagation properties of the edge states. Numerical results show that the surface termination along the ΓM direction can provide two edge states in the frequency region of interest. The feasibility of controlling the dispersion relation by subtle structural modification is investigated and compared for these two types of edge mode. Our results provide important theoretical basis for the potential application offered by the polyatomic photonic crystal in on-chip optical buffers and enhanced light matter interaction.

References

[1] ISHIZAKI K NODA S. Manipulation of photons at the surface of three-dimensional photonic crystals[J]. *Nature*, 2009, **460**(7253): 367-370.

[2] TIAN Shuang, TONG Yuan-wei. Effect of changing surface structure of photonic crystals on image[J]. *Acta Photonica Sinica*, 2013, **42**(2): 171-175.

[3] CAI Qing, HUANG Chang-qing, LIANG Pei, *et al*. Surface modes of two-dimensional photonic crystal based on plane wave expansion method[J]. *Acta Photonica Sinica*, 2012, **41**(4): 430-435.

[4] ŚMIGAJ W. Model of light collimation by photonic crystal surface modes[J]. *Physical Review B*, 2007, **75**(20): 205430.

[5] CAGLAYAN H, BULU I, OZBAY E. Off-axis directional beaming via photonic crystal surface modes[J]. *Applied Physics Letters*, 2008, **92**(9): 092114.

[6] CHEN H C, TSIA K K, POON A W. Surface modes in two-dimensional photonic crystal slabs with a flat dielectric margin [J]. *Optics Express*, 2006, **14**(16): 7368-7377.

[7] VLASOV Y A, MOLL N, MCNAB S J. Mode mixing in asymmetric double-trench photonic crystal waveguides[J]. *Journal of Applied Physics*, 2004, **95**(9): 4538-4544.

[8] VOLKOV V S, BOZHEVOLNYI S I, FRANDSEN L H, *et al*. Direct observation of surface mode excitation and slow light coupling in photonic crystal waveguides[J]. *Nano Letters*, 2007, **7**(8): 2341-2345.

[9] ZHANG Z, DAINESE M, WOSINSKI L, *et al*. Optical filter based on two-dimensional photonic crystal surface-mode cavity in amorphous silicon-on-silica structure[J]. *Applied Physics Letters*, 2007, **90**(4): 041108.

[10] WANG Jing, SONG Yi, YAN Wei, *et al*. High-Q photonic crystal surface-mode cavities on crystalline SOI structures[J]. *Optics Communications*, 2010, **283**(11): 2461-2464.

[11] YANG J K, KIM S H, KIM G H, *et al*. Slab-edge modes in two-dimensional photonic crystals [J]. *Applied Physics Letters*, 2004, **84**(16): 3016-3018.

[12] LU T W, LU S P, CHIU L H, *et al*. Square lattice photonic crystal surface mode lasers[J]. *Optics Express*, 2010, **18**(25): 26461-26468.

[13] LU T W, HSIAO Y H, HO W D, *et al*. High-index sensitivity of surface mode in photonic crystal het-ero-slab-edge microcavity[J]. *Optics Letters*, 2010, **35**(9): 1452-1454.

[14] PLOTNIK Y, RECHTSMAN M C, SONG D H, *et al*. Observation of unconventional edge states in 'photonic graphene'[J]. *Nature Materials*, 2014, **13**(1): 57-62.

[15] OUYANG Chun-fang, XIONG Zhi-qiang, ZHAO Fang-yuan, *et al*. Slow light with low group-velocity dispersion at the edge of photonic grapheme[J]. *Physical Review A*, 2011, **84**(1): 015801.

[16] KURT H, ERIM N, ÜSTÜN K. Slow light based on optical surface modes of two-dimensional photonic crystals [J]. *Journal of the Optical Society of America B*, 2012, **29**(6): 1187-1193.

[17] WANG Dao-bin, ZHANG Jie, YUAN Li-hua, *et al*. Slow light engineering in polyatomic photonic crystal waveguides based on square lattice[J]. *Optics Communications*, 2011, **284**(24): 5829-5832.

[18] MORRISON S K, KIVSHAR Y S. Tamm states and nonlinear surface modes in photonic crystals [J]. *Optics Communications*, 2006, **266**(1): 323-326.

[19] JOHNSON S G, JOANNOPOULOS J D. Block-iterative frequency-domain methods for Maxwell's equations in a planewave basis[J]. *Optics Express*, 2001, **8**: 173-190.

[20] MA Jing, JIANG Chun. Flatband slow light in asymmetric line-defect photonic crystal waveguide featuring low group velocity and dispersion [J]. *IEEE Journal of Quantum Electronics*, 2008, **44**(8): 763.

[21] HAO R, CASSAN E, ROUX X L, *et al*. Improvement of delay-bandwidth product in photonic crystal slow-light waveguides[J]. *Optics Express*, 2010, **18**(26): 16309.

[22] KURT H, ÜSTÜN K, AYAS L. Study of different spectral regions and delay bandwidth relation in slow light photonic crystal waveguides [J]. *Optics Express*, 2010, **18**(26): 26965.

[23] LI Xu, LE Zi-chun. The design and simulation of wavelength division demultiplexer based on photonic crystal micro-cavity [J]. *Acta Photonica Sinica*, 2014, **4**(s1): 0123003.